Protective human monoclonal antibodies that target the Type III Secretion System of Pseudomonas aeruginosa inhibit translocon function

Jean-Mathieu Desveaux, Eric Faudry, Carlos Contreras-Martel, François Cretin, Leonardo Sebastian Dergan-Dylon, Axelle Amen, Isabelle Bally, Victor Tardivy-Casemajor, Fabien Chenavier, Delphine Fouquenet, et al.

Protective human monoclonal antibodies that target the Type III Secretion System of *Pseudomonas aeruginosa* inhibit translocon function

Jean-Mathieu Desveaux[1], Eric Faudry[1], Carlos Contreras-Martel[1], François Cretin[1], Leonardo Sebastian Dergan-Dylon[1], Axelle Amen[1,2], Isabelle Bally[1], Victor Tardivy-Casemajor[1], Fabien Chenavier[1], Delphine Fouquenet[3], Yvan Caspar[1,4], Ina Attrée*[1], Andréa Dessen*[1], Pascal Poignard*[1]

[1] Univ. Grenoble Alpes, CEA, CNRS, Institut de Biologie Structurale (IBS), F-38044 Grenoble, France

[2] Laboratoire d'Immunologie, CHU Grenoble Alpes, France

[3]Centre d'Étude des Pathologies Respiratoires INSERM U1100 UFR de Médecine de Tours, 10 Bd Tonnellé, 37032 Tours Cedex

[4] Laboratoire de Bactériologie-Hygiène Hospitalière, CHU Grenoble Alpes, France

* to whom correspondence should be addressed: ina.attree@ibs.fr, andrea.dessen@ibs.fr, pascal.poignard@ibs.fr

ABSTRACT

Pseudomonas aeruginosa is a major human opportunistic pathogen associated with a high incidence of multi-drug resistance. The antibody-based blockade of *P. aeruginosa* virulence factors represents a promising alternative strategy to mitigate its infectivity. In this study, we employed single B cell sorting to isolate, from cystic fibrosis patients, human monoclonal antibodies (mAbs) targeting proteins from the *P. aeruginosa* Type 3 Secretion System (T3SS) and characterized a panel of mAbs directed at PscF and PcrV. Among those, two mAbs, P5B3 and P3D6, that bind to the injectisome tip protein PcrV, exhibited T3SS blocking activity. We solved the crystal structure of the P3D6 Fab-PcrV complex, which revealed that the Ab binds to the C-terminal region of PcrV. Further, we compared the T3SS-blocking activity of three PcrV-targeting mAbs, including two from previous independent studies, using two distinct assays to evaluate pore formation and toxin injection. We conducted a mechanistic and structural analysis of their modes of action through modeling based on the known structure of a functional homolog, SipD from *Salmonella typhimurium*. The analysis suggests that anti-PcrV mAbs may act through different mechanisms, ranging from preventing PcrV oligomerization to disrupting PcrV's scaffolding function, thereby inhibiting the assembly and function of the translocon pore. Our findings provide additional evidence that T3SS-targeting Abs, some capable of inhibiting virulence, are elicited in *P. aeruginosa*-infected patients. The results offer deeper insights into PcrV recognition by mAbs and their associated mechanisms of action, helping to identify which Abs are more likely to be therapeutically useful based on their mode of action and potency. This paves the way for developing effective alternatives to traditional antibiotics in the fight against this resilient pathogen.

INTRODUCTION

The emergence of antimicrobial resistance is a major threat to human health. Among the microorganisms whose resistance rates have increased the most dramatically are ESKAPE pathogens (***E****nterococcus faecium,* ***S****taphylococcus aureus,* ***K****lebsiella pneumoniae,* ***A****cinetobacter baumannii,* ***P****seudomonas aeruginosa,* ***E****nterobacter spp*) for which novel antibacterial treatments are urgently needed. However, an antibiotic discovery hiatus that occurred during the last few decades severely heightened the resistance threat (Murray et al., 2022), underlining the importance of exploring alternative strategies such as host-targeting, bacteriophage, anti-virulence, and Ab-based therapies (De Melo et al., 2024; Kaufmann et al., 2018; Morrison, 2015).

Therapeutic mAbs have been successfully developed to fight viral infections ranging from Ebola to SARS-CoV-2 (Crowe, 2022; Levin et al., 2022; Mulangu et al., 2019). To date, however, only three therapeutic Abs have been marketed against bacteria, all of which target toxins. Other types of bacterial virulence factors could also serve as potential high importance targets for mAbs. Recent examples include the development of mAbs that target lipopolysaccharides, O-antigen, and outer membrane transporter proteins, notably in *Klebsiella pneumoniae* and *Mycobacterium tuberculosis* (Pennini et al., 2017; Rollenske et al., 2018; Watson et al., 2021). The advantages of targeting virulence factors through mAbs include notably a high specificity and the decreased likelihood of the emergence of resistance among bacteria (La Guidara et al., 2024). Additionally, the employment of mAb engineering platforms offers the potential for improved efficacy through modifications such as half-life extension and alterations of Fc effector functions (Morrison, 2015; Vacca et al., 2022). Finally, strategies such as the use of mAb cocktails targeting different specificities and the combination with traditional antibiotics further expand the range of Ab-based treatment options (Duan et al., 2021; Morrison, 2015; Tabor et al., 2018).

Pseudomonas aeruginosa is a major nosocomial pathogen and the leading cause of acute pneumonia and chronic lung infections, particularly in ventilator-assisted and cystic fibrosis (CF) patients. Infections with *P. aeruginosa* ultimately lead to loss of lung function and death in CF patients. Worldwide, *P. aeruginosa* is responsible for more than 300,000 deaths associated or attributed to resistance each year. The natural resistance of *P. aeruginosa* to a broad range of antibiotics, its ability

to grow as biofilms, as well as its widespread presence in hospital settings (Horcajada et al., 2019; Murray et al., 2022), have called for urgent efforts towards the development of new therapeutic agents. Aggressive acute infections by *P. aeruginosa* are highly dependent on its Type III Secretion System (T3SS), a needle-like, multi-component secretion machinery located on the cell surface and that transports effectors from the bacterial cytoplasm directly into the host cell cytosol (Goure et al., 2004; Hauser, 2009; Quinaud et al., 2007, 2005). It is of note that in other human pathogens such as *Yersinia pestis*, *Salmonella typhi*, *Shigella dysenteriae* and *Escherichia coli* the T3SS also plays a key role in virulence, participating in the causation of diseases such as plague, typhoid fever, and bacillary dysentery, respectively (Coburn et al., 2007; Diepold and Wagner, 2014; Hu et al., 2017; Serapio-Palacios and Finlay, 2020).

A key component of the T3SS is the injectisome, membrane-embedded protein rings extended by a hollow needle, composed of the PscF protein that protrudes outwards from the bacterial surface. Injectisome-dependent toxin delivery, which occurs upon contact with the eukaryotic target cell, also requires formation of the 'translocon', a complex of three proteins that are exported through the interior of the polymerized needle, assemble at its tip and form a pore in the eukaryotic cell membrane, an essential step for effector injection (Mueller et al., 2008). The translocon is composed of two hydrophobic proteins (PopB and PopD in *P. aeruginosa*), as well as a hydrophilic partner - PcrV, or the V antigen- in *P. aeruginosa* (Matteï et al., 2011). PopB and PopD have been shown to act as *bona fide* pore-forming toxins (Schoehn et al., 2003; Faudry et al., 2006; Montagner et al., 2011) that, upon membrane disruption, can trigger the manipulation of host processes including histone dephosphorylation and mitochondrial network disruption (Dortet et al., 2018). PcrV, on the other hand, oligomerizes at the tip of the T3SS needle and aids PopB and PopD in their membrane disruption process (Gébus et al., 2009; Goure et al., 2005; Guo and Galán, 2021; Matteï et al., 2011). Crystal structures of monomeric homologs of PcrV (LcrV, SipD, BipD) have shown that they fold into an elongated coiled-coil buttressed by an α-helical hairpin at the N-terminus and an α/β carboxy-terminal region (Derewenda, 2011; Erskine et al., 2006; Lunelli et al., 2011). Notably, the cryo-EM structure of a needle filament complex composed of PrgI (needle protein) with SipD (tip protein) at its extremity confirmed that the latter forms a pentamer where the first

and fifth subunits are separated by a gap, thus generating a heterogeneous assembly (Guo and Galán, 2021). This arrangement could be similar in numerous T3SS systems (Habenstein et al., 2019).

Given the importance of the T3SS for *P. aeruginosa* infection, components such as PcrV and PscF have been explored as targets for the development of therapeutic Abs and inhibitory small molecules, respectively (Berube et al., 2017; Bowlin et al., 2014). Animal models have shown that blocking the T3SS, particularly the function of PcrV, can successfully diminish tissue damage due to *P. aeruginosa* infection (Frank et al., 2002; Imamura et al., 2007). Moreover, in ventilated patients, pegylated Fabs that target PcrV (KB001-A) were shown to successfully reduce the incidence of pneumonia, which is consistent with the role of T3SS in the acute phase of infection (Jain et al., 2018; Roy-Burman et al., 2001). However, this treatment did not benefit chronically colonized CF patients in terms of antibiotic needs (François et al., 2012; Jain et al., 2018; Yaeger et al., 2021). In addition, the bispecific MEDI3902 mAb targeting both PcrV and the Psl exopolysaccharide successfully protected against *P. aeruginosa* infection in animal models but was discontinued in phase II clinical trials (Chastre et al., 2022; DiGiandomenico et al., 2014). Nevertheless, PcrV remains an attractive target, motivating the search for potentially more effective Abs (Simonis et al., 2023).

Here, we sorted specific single memory B cells from peripheral blood mononuclear cells (PBMCs) of cystic fibrosis patients to identify mAbs against PcrV and PscF with potential T3SS-inhibiting activity. Two anti-PcrV mAbs (P5B3 and P3D6) showed inhibition of the injection of the T3SS effector ExoS into epithelial cells, with mAb P5B3 displaying blocking activity against five major PcrV variants representing more than 80% of clinical isolates sequenced to date. We obtained the crystal structure of a P3D6 Fab-PcrV complex and further compared the mechanisms of actions of different anti-PcrV mAbs targeting various epitopes, including one mAb from a recent publication (Simonis et al., 2023). These structure-based analyses of the mechanisms of action of the different mAbs provide valuable insights for the development of improved antipseudomonal treatments and preventive approaches.

RESULTS

Selection of donors exhibiting T3SS-inhibiting circulating IgG responses

Our approach was based on single cell sorting of recombinant PcrV and PscF specific memory B cells from human donor peripheral blood mononuclear cells (PBMCs). To identify donors with anti-PcrV and -PscF mAbs with T3SS-inhibitory activity, we first evaluated in ELISA the reactivity of sera from a cohort of CF patients that were chronically colonized with *P. aeruginosa* against recombinant PcrV and PscF before testing them in functional assays (Figure 1A). Among the 34 sera tested, donors 16 and 25 exhibited the strongest reactivity for both proteins (Figure 1B).

To assess the capacity of serum-purified IgGs to block T3SS effector translocation, we used a previously developed cellular model that is based on the T3SS-dependent translocation of the ExoS effector fused to β-lactamase, ExoS-Bla (Verove et al., 2012). Briefly, epithelial cells were exposed to *P. aeruginosa* CHAΔ*exoS* expressing the ExoS-Bla reporter in the presence of patients' polyclonal purified IgGs. ExoS-Bla translocation was measured by monitoring fluorescence of the β-lactamase FRET-competent substrate CCF2-AM, and expressed as normalized reporter injection. Polyclonal IgGs from donors 16 and 25 showed a potent ExoS-Bla translocation blocking activity with an almost complete inhibition of injection at 160 µg/mL (Figure 1C). To investigate whether the observed activity was driven by anti-PcrV and/or anti-PscF specific IgGs, we absorbed specific Abs on beads coated with recombinant PcrV or PscF to obtain polyclonal IgG samples depleted of the corresponding specific IgGs (Figure 1D, top). The T3SS blocking activity of depleted polyclonal IgGs was then evaluated using the same method as above (Figure 1D, bottom). The results showed a decrease in inhibitory activity when anti-PcrV Abs were depleted from donor 25's IgGs and when anti-PscF Abs were depleted from donor 16's IgGs, suggesting the presence of inhibitory Abs against the respective proteins. Additionally, the findings demonstrated that our recombinant antigen baits could effectively bind T3SS-inhibitory Abs and could therefore be used to isolate memory B cells producing the corresponding IgGs.

Isolation of PcrV and PscF mAbs using a single cell direct sorting approach

To isolate mAbs specific to PcrV and PscF, PBMCs were purified from whole blood from the two selected donors. Next, using single cell sorting, IgG positive memory B cells were isolated based on their ability to recognize either PscF or PcrV (Figure 2A) and seeded at the frequency of one cell per well. Variable heavy and light chain gene sequences were retrieved from isolated B cells leading to the production of a total of 66 recombinant mAbs (53 and 13 putative anti-PscF and anti-PcrV, respectively). The specific binding capacities of 10 anti-PscF and 4 anti-PcrV mAbs were confirmed by ELISA against the corresponding recombinant proteins. EC_{50} values calculated from ELISA data showed variable apparent affinities ranging from ~50 µg/mL to 0.02 µg/mL (Figure 2B). Isolated mAbs originated from a variety of variable gene germline families, as determined using the international immunogenetics information system (IMGT) database alignments, and did not present any notable features in term of mutation rates or HCDR3 length (Supplementary Table 1), with no particular enrichment noted.

The ability of ELISA-confirmed anti-PscF and anti-PcrV mAbs to block T3SS-mediated activity at a concentration of 100 µg/mL was subsequently evaluated using the ExoS-Bla reporter system. No significant reduction in ExoS-Bla injection was observed for any of the anti-PscF mAbs tested. However, two out of four anti-PcrV mAbs, P5B3 and P3D6, significantly reduced ExoS-Bla injection, with P3D6 displaying significantly stronger efficacy (Figure 2B).

To map the epitopes of the isolated mAbs, we next performed competition ELISAs (Supplementary Table 2). Antibodies directed at PscF grouped into three clusters, with P1D8 and P5G10 mAbs competing only against themselves. Similarly, anti-PcrV mAbs also grouped into three clusters, with the two anti-PcrV mAbs exhibiting T3SS inhibitory activity, P5B3 and P3D6, seemingly targeting overlapping epitopes. Precise affinities of both mAbs were measured using biolayer interferometry (BLI), revealing subnanomolar K_D values (Supplementary Table 3). Notably, P3D6 exhibited approximately 30-fold lower affinity compared to P3B3, despite demonstrating greater efficacy in the inhibitory assay.

P5B3 inhibits T3SS-dependent toxin injection by recognizing a highly conserved epitope of PcrV

Polymorphism in PcrV protein sequences was reported among *P. aeruginosa* clinical isolates and should be considered in the development of therapeutic human monoclonal Abs targeting PcrV (Figure 3A) (Tabor et al., 2018). To determine whether the blocking activity of mAbs P5B3 and P3D6 was impacted by the PcrV sequence, the reporter ExoS-Bla was introduced into a strain that lacked isogenic PcrV (Δ*pcrV*) and synthetized the five most prevalent PcrV variants found in over 80% of clinical isolates (Tabor et al., 2018). Monoclonal Ab P5B3 showed statistically significant T3SS blocking activity towards all variants (Figure 3B) with estimated IC_{50} values of 100 μg/ml for variants 1, 2, 3, 4 and 400 μg/ml for variant 5 (Supplementary Figure 1). In contrast, mAb P3D6 had no effect on variants 2, 3, 4 and 5, but strongly inhibited variant 1 (Figure 3B) with an estimated IC_{50} of 3.7 μg/ml (Supplementary Figure 1), indicating that the epitope recognized by P3D6 differs between PcrV variants.

Anti-PcrV mAbs block translocon pore assembly

It has been suggested that PcrV scaffolds the assembly of the PopB/PopD translocon within host membranes by interacting with the PopD component of the pore (Goure et al., 2004; Kundracik et al., 2022, 2022; Matteï et al., 2011). Furthermore, polyclonal Abs raised against PcrV have been shown to inhibit the assembly of the translocon in target membranes (Goure et al., 2005).

To investigate the mechanistic details of the inhibitory activity of mAbs P3D6 and P5B3, we used a *P. aeruginosa* strain deprived of all three T3SS effectors, ExoS, ExoT and ExoY. This strain, named PAO1Δ3Tox (Cisz et al., 2008) harbors PcrV variant 1 and provokes toxin-independent macrophage pyroptosis upon membrane insertion of the PopB/PopD translocation pore (Dacheux et al., 2001). Death of J774 macrophages was monitored during 4h post-infection by measuring an increase in propidium iodide fluorescence due to DNA binding to the nuclei of dead cells. Both mAbs significantly reduced the cytotoxicity induced by PAO1Δ3Tox by 28% and 73%, respectively (Figure 4A). Monoclonal Ab P3D6 exhibited a dose-response inhibition with an estimated IC_{50} of 11.8 μg/mL (Figure 4B), while P5B3 did not exhibit a

246 significant dose-response effect at concentrations below 100 µg/mL (Figure 4C).
247 Overall, these results indicate that the binding of both mAbs to PcrV reduces the
248 formation of the translocation pore in target cell membranes, with P3D6 exhibiting more
249 potent activity.

250

251 **Crystal structure of PcrV* bound to Fab P3D6**

252 In order to identify the PcrV epitopes recognized by the two mAbs, we generated
253 a plasmid encoding a form of PcrV (PcrV*) amenable to crystallization (Tabor et al.,
254 2018) as well as Fab fragments from both P3D6 and P5B3 mAbs. PcrV* was
255 expressed in *E. coli* while both Fabs were expressed in HEK293F cells. Individual
256 proteins were purified by affinity and size-exclusion chromatographies. PcrV* was
257 incubated with either Fab fragment and samples were co-purified using size exclusion
258 chromatography. Despite the fact that both PcrV*-Fab P3D6 and PcrV*-Fab P5B3
259 complexes co-eluted in gel filtration, only the PcrV*-Fab P3D6 complex subsequently
260 generated diffracting crystals. Data were collected at the ESRF synchrotron in
261 Grenoble and the structure was solved by molecular replacement using Phaser
262 (McCoy et al., 2007). Iterative manual model building and model improvement led to
263 the structure whose statistics for data collection and refinement are presented in
264 Supplementary Table 4.

265 PcrV* is composed of six helices interwoven by loop regions. α-helices 1, 4 and
266 6 are the major secondary structure elements in PcrV*, while helices 2, 3 and 5 are 1-
267 or 2-turn helices. Most of the contacts formed between PcrV* and Fab P3D6 involve
268 Helix 6 and the loop preceding it (Figures 5A, 5B) and implicate a binding platform
269 made by both LC and HC from Fab P3D6. From the PcrV side, the interaction region
270 is highly polar, being formed by the side chains of Lys208, Gln217, Glu220, Lys222,
271 Ser225, Asp 226, Tyr 228, Glu231, Asn234, Thr243, Asp246 and Arg247. The
272 substitution of Ser225 in PcrV variant V1 by Lys or Arg in variants V2 to V5 is consistent
273 with P3D6 being inefficient on strains harboring these four variants.

274 In order to understand the protective role of mAb P3D6 in the context of the
275 PcrV pentameric oligomer located at the tip of the PscF needle, we generated a model
276 using the cryo-EM structure of the SipD pentamer (Guo and Galán, 2021) and aligned
277 our co-crystal structure onto this model (Figures 5C, 5D).This analysis revealed that

Fab P3D6 can successfully bind to one PcrV monomer (dark red and orange in Figure 5, respectively), but would be unable to bind to a pre-formed PcrV pentamer due to the generation of clashes with neighboring subunits of the oligomeric form (Figure 5; the structure of the Fab can be seen overlaid with that of the pentamer subunits).

DISCUSSION

We generated a panel of anti-PscF and -PcrV human mAbs through specific memory B cell sorting from selected individuals. Although adsorption experiments with recombinant PscF suggested the presence of anti-PscF Abs with T3SS inhibitory activity in the donor from whom they were isolated, none of the isolated mAbs exhibited this activity. Competition mapping showed that the anti-PscF mAbs targeted three distinct regions of PscF, none of which seemingly involved in inhibitory activity. Further epitope mapping would be necessary to gain deeper insight; however, in the absence of a PscF structure, this remains challenging. Isolating a greater number of mAbs from a selected donor with strong anti-PscF inhibitory activity would certainly increase the likelihood of identifying one with T3SS-inhibiting properties.

Of the four anti-PcrV mAbs isolated, two exhibited T3SS inhibitory capacity. Their mechanism of action could potentially involve (i) prevention of effector secretion by acting as a cap for PcrV; (ii) prevention of effector translocation towards the host cell by disruption of the PcrV-PopB/PopD interaction; or (iii) prevention of oligomerization of PcrV itself(Gébus et al., 2009; Sawa et al., 2019). Here, we measured the ability of the inhibiting anti-PcrV mAbs we isolated to block PopB/PopD pore formation and toxin injection, and carried out a mechanistic and structural analysis of their activity, in parallel with other mAbs targeting PcrV.

We set out to investigate and compare the mechanism of action of several anti-PcrV mAbs: P3D6 mAb and P5B3 (this work), 30-B8 (Simonis et al., 2023), as well as a previously reported humanized, bivalent PcrV-Psl mAb (DiGiandomenico et al., 2014). In order to do so, we produced mAb 30-B8 and subsequently purchased mAb MEDI3902 from MedChem. The P3D6, P5B3, 30-B8 and MEDI3902 mAbs were notably compared by employing two assays capable of detecting T3SS inhibition, each with a different readout: injection of the ExoS-Bla reporter into epithelial cells and cytotoxicity measurements in macrophages as a read-out for translocon assembly. In

addition, we performed structural analyses on three of the mAb-PcrV complexes, from the viewpoints of recognition of both monomeric and pentameric forms of PcrV.

Both MEDI3902 and 30-B8 mAbs potently inhibited the injection of ExoS-Bla into target cells, with IC_{50} values of 117 ng/ml and 21.3 ng/ml, respectively (Figure 6A). Monoclonal Abs isolated in this study also inhibited toxin injection, although significantly less potently, with IC_{50} values of 3.65 µg/mL for P3D6, and around 100 µg/mL for P5B3. Monoclonal Ab MEDI3902 had previously been shown to bind to different PcrV variants (Tabor et al., 2018) and here we confirmed that mAb 30-B8 was similarly efficient at inhibiting toxin injection by strains carrying five different PcrV variants (Simonis et al., 2023) (Supplementary Figure 2). Monoclonal Ab P5B3 was also able to inhibit all variants, but only at high concentrations, while P3D6 was only active against variant V1. Therefore, P5B3 appears to recognize a highly conserved epitope whereas P3D6 seems to bind an overlapping epitope that includes the variable Ser225, as suggested by the ELISA mapping competition and structural data, but does so in a more effective manner.

In the macrophage cytotoxicity assay, translocon assembly was inhibited by mAbs 30-B8 (IC_{50} of 45.2 ng/ml) and P3D6 (IC_{50} of 11.8 µg/mL), while P5B3 and MEDI3902 did not exhibit significant dose-response inhibition. Together, these results suggest that the T3SS-inhibiting activity of these anti-PcrV Abs may occur through distinct mechanisms.

In order to understand the differences in potency and potentially in mechanisms of action at a structural level, we compared the Fab-PcrV interaction regions for the P3D6, 30-B8 and MEDI3902 Fabs. Monomeric PcrV is an elongated, dumbbell-shaped molecule, and the chimeric form used in this study displays the same characteristics (Figure 5A). Fab MEDI3902 binds to one of the extremities of monomeric PcrV, extending in the longitudinal axis of the molecule (Figure 6B, top). This mode of binding is distinct from that of 30-B8 and P3D6 Fabs, both of which recognize the C-terminal region of PcrV (Figure 6B, middle) (Simonis et al., 2023). Therefore, the binding region of 30-B8 and P3D6 does not, by itself, appear to explain the significant difference in potency between the two mAbs. Moreover, a difference in affinity does not account for the difference in potency either, as both mAbs bind to recombinant monomeric PcrV with comparable apparent affinities of around 30 ng/ml (our data and Simonis et al., 2023).

In order to perform this comparative analysis in the context of a PcrV oligomer, we employed the model of the PcrV pentamer generated as described above, which was based on the cryo-EM structure of SipD from *S. typhimurium* (Guo and Galán, 2021). According to this analysis, the only Fab that is able to bind to all PcrV protomers in the pentamer without generating clashes with either PcrV or other Fabs is 30-B8 (Figure 6). In the case of MEDI3902, the Fab can bind the oligomer, but only with a 1:5 stoichiometry, due to possibility of clashes between Fabs. Finally, P3D6 is unable to bind to a pre-formed pentamer, and can only recognize a PcrV protomer in its monomeric form.

This structural analysis suggests different potential mechanisms of action. For P3D6, the inability to bind to the pentamer points towards a mechanism involving inhibition of oligomerization. Indeed, the analysis shows that binding of P3D6 to a single PcrV monomer prevents the association of additional PcrV protomers through Fab-protomer direct clashes. A similar mechanism of action may be suggested for MEDI3902, as Fab-bound PcrV protomers cannot oligomerize, in this case due to clashes between the Fabs themselves (Fig. 6). However, the fact that MEDI3902 does not appear to prevent translocon insertion suggests that such a mechanism is unlikely for this mAb as PcrV oligomerisation is required at the tip of the needle for translocon assembly. In contrast to P3D6, MEDI3902 can bind the oligomerized PcrV pentamer (with a stoichiometry of one) and its mechanism of action may thus be related to this ability. Our results suggest that when MEDI3902 is bound to the PcrV oligomer, the formation of the pore is not efficiently blocked while toxin injection is strongly inhibited (Fig. 6). Therefore, the presence of one MEDI3902 Ab molecule at the tip of the needle does not appear to efficiently prevent either the secretion of the translocator proteins PopB/PopD through the needle, nor the interactions between PcrV and PopB/PopD, which have been described as required for pore formation (Kundracik et al., 2022). However, the MEDI3902 Ab molecule, seems to interfere with further interactions between PcrV and the PopB/PopB complex, or with the sensing by PcrV of the host cell, both of which are needed for toxin injection (Lee et al., 2010).

Lastly, 30-B8, which can bind the formed pentamer with a stoichiometry of five, appears to be the most effective at blocking both pore formation and toxin injection. The fact that the PcrV-bound 30-B8 Ab probably projects towards the cell membrane,

associated with its ability to bind to the PcrV pentamer at full occupancy, may result in remarkable efficacy in blocking the interactions between PcrV and PopB/PopD.

In conclusion, here we show that patients with chronic infection with *P. aeruginosa* can elicit anti-PscF and anti-PcrV mAbs that recognize different regions within these proteins. Anti-PcrV Abs can act as T3SS inhibitors through different mechanisms, with some exhibiting significantly greater efficacy than others. The strategy employed here, involving the analysis of structural and functional data on anti-T3SS mAbs should open new avenues towards deciphering the mechanism of T3SS toxin translocation and enable the isolation of more effective mAbs targeting a broad range of clinical strains.

MATERIALS and METHODS

Clinical sample collection

The study was approved by the French ethics committee (ID-RCB 2020-A00311-38) and was carried out according to the Declaration of Helsinki, Good Clinical Practice (GCP) guidelines and current French regulations. Written consent for participation was not required for this study. The first phase was a non-interventional study involving data and samples from human participants conducted according to Reference Methodology No. 004 issued by French authorities (Commission Nationale de l'Informatique et des Libertés). Screening and functional assays were performed on human sera previously collected at Grenoble Alpes University Hospital (France), from CF patients chronically infected with *P. aeruginosa*. Participants were all informed and did not object to this phase of the study. Inclusion criteria for the second phase of the study were: patients with positive screening during phase one, ≥ 18 years old, ≥32 Kg, with a programmed blood sampling at Grenoble Alpes University Hospital and not being opposed to the second phase of the project. Whole blood was then collected using BD Vacutainer® EDTA tubes (Becton Dickinson) and PBMCs were purified by density gradient centrifugation using Lymphoprep (Eurobio scientific) following manufacturing guidelines. Cells were then stored in liquid nitrogen until further use.

Bacterial strains, genetic manipulations and growth conditions

P. aeruginosa strains used in this study are listed in Supplementary Table 5. Strains were cultured in LB media at 37 °C. For infection experiments, bacteria were grown until the measured optical density at 600 nm (OD_{600nm}) of 1. The genes encoding the most common variants of PcrV were cloned into the *Pseudomonas* replicative vector derived from pUCP21 (West et al., 1994) containing the P*pcrG* promoter driving the *pcrGVHpopDB* operon expression (West et al., 1994). The plasmids, kindly provided by Simona Barzu (Sanofi Pasteur, Lyon), were transformed into the *P. aeruginosa* strain CHA lacking *pcrV* (Goure et al., 2004).

Expression and purification of full length PcrV and PcrV*

Expression of full-length PcrV from strain PAO1, cloned into a pET15b vector, was performed in *E. coli* BL21(DE3) as previously described, with small modifications (Nanao et al., 2003). Expression was induced with 1mM of Isopropyl β-D-1-thiogalactopyranoside (IPTG) at OD_{600} = 0.8 AU and cells were then grown overnight at 20°C with shaking at 250 rpm. Cells were harvested by centrifugation and lysed by passing through a French Press 3 times at 25 Kpsi in lysis Buffer (50 mM Tris pH8, 200 mM NaCl, 20 mM Imidazole) supplemented with a protein inhibitor cocktail tablet (ROCHE). The supernatant was cleared by centrifugation at 18,000 rpm and subsequently loaded onto Ni-IDA resin (Macherey-Nagel). The resin was washed with lysis buffer and the sample was eluted with lysis buffer supplemented with 100 mM imidazole. Fractions containing the sample were pooled and applied to a size-exclusion chromatography column (Superdex 200 HiLoad 16/600) pre-equilibrated in SEC buffer (20mM Tris pH 8, 150 mM NaCl, 1 mM EDTA). A chimeric form of PcrV (PcrV*) consisting of amino acids 1-17 fused to 136-249, was constructed based on a construct made by Tabor et al. (2018) and employed for crystallization purposes. The purification protocol was the same as above, the only difference being that 250 mM imidazole was employed to elute the sample from the Ni resin.

Expression and purification of PscF

Expression of PscF from strain PAO1 was performed in *E. coli* BL21(DE3) grown in Terrific Broth. Expression was induced with 1 mM Isopropyl β-D-1-thiogalactopyranoside (IPTG) at OD_{600} = 0.6 AU and cells were then grown for an

additional 3 hours at 37 °C with shaking at 250 rpm. Cells were harvested by centrifugation and lysed by passing through a French Press 3 times at 25 kpsi in lysis buffer (50 mM Tris pH 8, 200 mM NaCl, 20 mM Imidazole, 2 % glycerol) supplemented with a protein inhibitor cocktail tablet (Roche). The supernatant was cleared by centrifugation at 18,000 rpm and applied to a Ni-IDA resin (Macherey-Nagel). The resin was washed with lysis buffer and the protein was eluted with lysis buffer supplemented with 250 mM imidazole. Fractions were then buffer exchanged in an Amicon Ultra 10 kDa cutoff concentrator against a buffer exempt of imidazole (50 mM Tris pH 8, 200 mM NaCl, 2 % glycerol).

ELISA assays

For direct ELISA assays, serial dilutions of sera or mAbs were transferred in antigen-adsorbed wells of 96-well plates. Antigen binding was detected by an alkaline phosphatase-conjugated goat anti-human immunoglobulin G (IgG) F(ab′)2 Ab (Jackson Immuno). For competition ELISA, serial dilution of competitor mAbs were transferred in antigen-adsorbed wells. Following an incubation of 30 min, biotinylated mAbs were added to the wells at a concentration corresponding to the EC_{70} (Effective concentration 70). Biotinylated mAbs were detected using alkaline phosphatase conjugated streptavidin. Polyclonal Abs raised in rabbits against PscF and PcrV (Goure et al., 2004) were used as positive controls.

Sorting of specific memory B cells

Briefly, PBMCs were stained for 30 min at 4ºC in the dark, using Facs-Buffer (PBS-1X 0,5 % BSA , 2mM EDTA) with Live Dead staining (Thermo L34957), Anti-human CD3-Vio-Blue (Miltenyi 130-114-519), Anti-human CD20 Pe-Vio707 (Miltenyi 130-111-345), Anti-human CD19 Pe-Vio707 (Miltenyi 130-113-649), Anti-human IgM PE (Miltenyi 130-093-075), Anti-human IgA PE (Miltenyi 130-113-476), Anti-human IgD PE (Miltenyi 130-110-643), Anti-human CD27 APC (Miltenyi 130-108-336), in the presence of recombinant biotinylated His-PcrV-Avitag coupled with streptavidin BUV737 (BD 612775) or streptavidin Vio-515 (Miltenyi 103-107-459), and recombinant biotinylated His-PscF-Avitag coupled with streptavidin BUV496 (BD

612961) or streptavidin BV605 (Biolegend 405229). After washing, the cells were resuspended in Facs-Buffer and PscF or PcrV positive B cells are sorted and clonally seeded in 96 plates containing lysis buffer using BD FACSAria Fusion cytometer (BD Biosciences).

Isolation and production of mAbs

Sequences coding for variable regions of both heavy and light (κ and λ) chains were isolated by reverse transcription on total mRNA followed by a multiplex nested PCR using a set of primers covering the diversity of V-region diversity. V-regions family was attributed after sequencing of amplicons and alignment in the IMGT database (https://imgt.org). An additional round of PCR using primers specific to the identified family was performed followed by the cloning of V-regions genes in corresponding vectors containing IgG1H, IgGκ and IgGλ constant regions. MAbs were recovered by transient transfection in HEK293F cells (ThermoFisher scientific) and purification by affinity chromatography using Protein A Sepharose (Sigma). Regarding 30-B8, the sequences coding for the variable regions of heavy and light chains were synthesized by Eurofins according to the sequence published by Simonis and coworkers (Simonis et al., 2023). Cloning and production were performed as described above.

P3D6 and P5B3 Fab production

Sequences coding for Fab fragments were obtained by inserting stop codons on genes corresponding to heavy chains of the mAbs by PCR using site directed mutagenesis (Quickchange II, Agilent) according to manufacturer's instructions. Mutated heavy and corresponding light chain genes were cloned into appropriate expression plasmids for eukaryotic cell expression and were co-transfected at a 2:1 ration into FreeStyle 293-F cells (ThermoFisher). Fabs were purified using KappaSelect affinity chromatography (Cytiva).

Cellular tests for T3SS activity

ExoS-Bla translocation

The T3SS-dependent toxin injection into epithelial A549 cells was measured using the reporter system based on Bla/CCF2 enzyme/substrate combination (Charpentier and Oswald, 2004) previously described for *P. aeruginosa* (Verove et al., 2012). *P. aeruginosa* strain CHAΔ*exoS* carring ExoS-Bla fusion on the chromosome was used to infect A549 cells at the multiplicity of infection (MOI) of 5. The level of injected ExoS-β-lactamase was measured using CCF2 substrate, as described previously (Verove et al., 2012). All values were normalized using non-infected cells and cells infected in the absence of Abs as references.

Pore formation / propidium iodide incorporation into macrophages

To assess the formation of a T3SS translocation pore, macrophages were infected with a *P. aeruginosa* strain PAO1Δ3Tox devoid of three exotoxins (Cisz et al., 2008). Two days before the experiment, J774 cells were seeded in a 96-well plate (Greiner, 655090) at a density of 100 000 cells per well in DMEM supplemented with 10% FCS. The day before the experiment, the strain was grown overnight in LB medium. The next day, bacteria were sub-cultures in fresh LB media until an OD_{600nm} of 1 and the macrophages were washed two times with PBS before addition of 65 µL of DMEM 10% FCS containing 2 µg/mL of Propidium Iodide. Antibodies diluted in DMEM, 10% FCS (25 µL) were then added followed by 10 µL of bacteria diluted in DMEM 10% FCS to give a MOI of 5. Propidium iodide fluorescence was recorded in a Fluoroskan fluorimeter every 10 minutes. The data of each fluorescence kinetics of the triplicates were processed in R Studio to calculate the Area Under the Curve, as described before (Ngo et al., 2019). This metrics was then normalized using non-infected cells and cells infected in the absence of Abs as references.

Data processing and analysis

Data from independent cell experiments were pooled and analyzed in R Studio by one-way ANOVA followed by paired t-test or Kuskal-Wallis followed by the Dunn test. Dose-response fitting was performed using the drc package and logistic models.

Bio-layer interferometry

BLI experiments were performed on an OctetRED96e from Satorius/FortéBio (former Pall/FortéBio) and were recorded with software provided by the manufacturer

(Data Acquisition v11.1). All protein samples were diluted in analysis buffer (1X PBS pH 7.4, 0.02% Tween-20). 10 mM glycine pH 2.0 was used as regeneration buffer. Commercial SA or SAX (streptavidin) biosensors (Pall/FortéBio) were used to capture biotinylated PcrV. Kinetic analyses were performed in black 96-well plates (Nunc F96 MicroWell, Thermo Fisher Scientific) at 25°C with agitation at 1000 rpm. After incubation and equilibration of biosensors in analysis buffer, PcrV samples were applied at a concentration of 2.5 mg/ml by dipping biosensors until reaching a spectrum shift between 1.2 and 2 nm, followed by an additional equilibration step in analysis buffer. For association measurements, all analyte samples were diluted in analysis buffer at concentrations either between 3.12 and 200 nM for IgGs or between 50 and 3200 nM for Fab fragments. Association phases were monitored while dipping the functionalized biosensors in analyte solutions for 5 min after recording a baseline for 2 min, and the dissociation phases monitored in analysis buffer for 10min. To assess and monitor unspecific binding of analytes, measurements were performed with biosensors treated with the same protocols but replacing ligand solutions with analysis buffer. All measurements were performed in duplicate using sample preparations. Kinetic data were processed with software provided by the manufacturer (Data analysis HT v11.1). Signals from zero-concentration samples were subtracted from the signals obtained for each functionalized biosensor and each analyte concentration. Resulting specific kinetics signals were then fitted using a global fit method and 1:2 bivalent analyte model for full Abs/IgG and 1:1 Langmuir model for Fab. Reported kinetics parameter values were obtained by averaging the values obtained with duplicated assays and reported errors as the standard deviation.

Crystallization of the PcrV*-Fab P3D6 complex

PcrV* and P3D6 Fab were mixed in a 1:2 ratio for 1 hr at room temperature prior to being subjected to size exclusion chromatography using a Superdex 200 10/300GL increase column in SEC buffer (20 mM Tris pH 7.4, 150 mM NaCl, 1 mM EDTA). Peaks harboring PcrV*:Fab complexes in SDS-PAGE were pooled, concentrated and used for crystallization trials using the ISBG HTX crystallization platform in Grenoble. Initial crystallization conditions were optimized manually (25 % PEG 1000, 1mM $ZnCl_2$, 100 mM sodium acetate pH 5.5), and diffracting crystals were obtained using microseeding. All crystals were grown using the hanging drop vapor diffusion method at 20 °C. Single

crystals were mounted in cryo-loops and flash cooled in liquid nitrogen. X-ray diffraction data were collected under a nitrogen stream at 100° K at the European Synchrotron Facility (ESRF, Grenoble, France).

Structure determination and refinement

The best diffraction data were collected to 2.56 Å on beamline ID30A-1 (ESRF) (Bowler 2015). The diffracting crystal was in space group $P2_1$ and displayed one 1:1 PcrV:Fab complex per asymmetric unit. Statistics on data collection and refinement are summarized in supplementary table 5. X-ray diffraction images were indexed and scaled with XDS (Kabsch 2010). ADXV ("Arvai, A. (2020). ADXV. A Program to Display X-ray Diffraction Images. https://www.scripps.edu/tainer/arvai/adxv.html," n.d.) and XDSGUI (Brehm et al., 2023) were used to perform data quality and resolution cutoff check-ups (Karplus and Diederichs, 2015). The maximum possible resolution was determined using the STARANISO server (Tickle, 2007). The reduced X-ray diffraction data was imported into the CCP4 program suite (Agirre et al., 2023). The PcrV*-Fab P3D6 structure was solved by molecular replacement using PHASER (McCoy et al., 2007) and an AlphaFold2 ColabFold-generated model (Mirdita et al., 2022). The PcrV* and Fab model chains were placed sequentially. The structure was completed by cycles of manual model building with COOT (Emsley and Cowtan, 2004, p. 200). Water molecules were added to the residual electron density map as implemented in COOT. Crystallographic macromolecular refinement was performed with REFMAC (Murshudov et al., 2011). Cycles of model building and refinement were performed until R_{work} and R_{free} converged. The TLS definition was determined and validated using the TLSMD (Painter and Merritt, 2006) and PARVATI (Zucker et al., 2010) servers. The stereochemical quality of the refined models was verified with MOLPROBITY (Chen et al., 2010, p. 20), PROCHECK (Laskowski et al., 1993) and PDB-REDO (Joosten et al., 2014). Secondary structure assignment was performed by DSSP (Kabsch and Sander, 1983) and STRIDE (Heinig and Frishman, 2004). Figures displaying protein structures were generated with PYMOL (http://www.pymol.org).

ACKNOWLEDGEMENTS

This work was supported by a grant from the Agence Nationale de la Recherche (ANR-22-CE18-0009) to PP, AD and IA, as well as grant 183360 from the Région Auvergne Rhône-Alpes to PP and AD. This work used the platforms of the Grenoble Instruct-ERIC center (ISBG; UAR 3518 CNRSCEA-UGA-EMBL) within the Grenoble Partnership for Structural Biology (PSB), supported by FRISBI (ANR-10-INBS-0005-02) and GRAL, financed within the University Grenoble Alpes graduate school (Ecoles Universitaires de Recherche) CBH-EUR-GS (ANR-17-EURE-0003). The IBS acknowledges integration into the Interdisciplinary Research Institute of Grenoble (CEA).

DATA AVAILABILITY

All data generated or analyzed during this study are included in the manuscript and supporting files, with the exception of the final refined model coordinates and structure factors corresponding to the PcrV*- Fab P3D6 complex. Those were deposited in the Protein Data Bank (PDB, http://www.rcsb.org), ID code: 9FM0.

REFERENCES

Agirre J, Atanasova M, Bagdonas H, Ballard CB, Baslé A, Beilsten-Edmands J, Borges RJ, Brown DG, Burgos-Mármol JJ, Berrisford JM, Bond PS, Caballero I, Catapano L, Chojnowski G, Cook AG, Cowtan KD, Croll TI, Debreczeni JÉ, Devenish NE, Dodson EJ, Drevon TR, Emsley P, Evans G, Evans PR, Fando M, Foadi J, Fuentes-Montero L, Garman EF, Gerstel M, Gildea RJ, Hatti K, Hekkelman ML, Heuser P, Hoh SW, Hough MA, Jenkins HT, Jiménez E, Joosten RP, Keegan RM, Keep N, Krissinel EB, Kolenko P, Kovalevskiy O, Lamzin VS, Lawson DM, Lebedev AA, Leslie AGW, Lohkamp B, Long F, Malý M, McCoy AJ, McNicholas SJ, Medina A, Millán C, Murray JW, Murshudov GN, Nicholls RA, Noble MEM, Oeffner R, Pannu NS, Parkhurst JM, Pearce N, Pereira J, Perrakis A, Powell HR, Read RJ, Rigden DJ, Rochira W, Sammito M, Sánchez Rodríguez F, Sheldrick GM, Shelley KL, Simkovic F, Simpkin AJ, Skubak P, Sobolev E, Steiner RA, Stevenson K, Tews I, Thomas JMH, Thorn A, Valls JT, Uski V, Usón I, Vagin A, Velankar S, Vollmar M, Walden H, Waterman D, Wilson KS, Winn MD, Winter G, Wojdyr M, Yamashita K. 2023. The *CCP* 4 suite: integrative software for macromolecular crystallography. *Acta Crystallogr D Struct Biol* **79**:449–461. doi:10.1107/S2059798323003595

Arvai, A. (2020). ADXV. A Program to Display X-ray Diffraction Images. https://www.scripps.edu/tainer/arvai/adxv.html. n.d.

Berube BJ, Murphy KR, Torhan MC, Bowlin NO, Williams JD, Bowlin TL, Moir DT, Hauser AR. 2017. Impact of Type III Secretion Effectors and of Phenoxyacetamide Inhibitors of Type III Secretion on Abscess Formation in a Mouse Model of Pseudomonas aeruginosa Infection. *Antimicrob Agents Chemother* **61**:e01202-17. doi:10.1128/AAC.01202-17

Bowlin NO, Williams JD, Knoten CA, Torhan MC, Tashjian TF, Li B, Aiello D, Mecsas J, Hauser AR, Peet NP, Bowlin TL, Moir DT. 2014. Mutations in the Pseudomonas aeruginosa Needle Protein Gene *pscF* Confer Resistance to Phenoxyacetamide Inhibitors of the Type III Secretion System. *Antimicrob Agents Chemother* **58**:2211–2220. doi:10.1128/AAC.02795-13

Brehm W, Triviño J, Krahn JM, Usón I, Diederichs K. 2023. *XDSGUI* : a graphical user interface for *XDS* , *SHELX* and *ARCIMBOLDO*. *J Appl Crystallogr* **56**:1585–1594. doi:10.1107/S1600576723007057

Charpentier X, Oswald E. 2004. Identification of the Secretion and Translocation Domain of the Enteropathogenic and Enterohemorrhagic *Escherichia coli* Effector Cif, Using TEM-1 β-Lactamase as a New Fluorescence-Based Reporter. *J Bacteriol* **186**:5486–5495. doi:10.1128/JB.186.16.5486-5495.2004

Chastre J, François B, Bourgeois M, Komnos A, Ferrer R, Rahav G, De Schryver N, Lepape A, Koksal I, Luyt C-E, Sánchez-García M, Torres A, Eggimann P, Koulenti D,

650 Holland TL, Ali O, Shoemaker K, Ren P, Sauser J, Ruzin A, Tabor DE, Akhgar A, Wu
651 Y, Jiang Y, DiGiandomenico A, Colbert S, Vandamme D, Coenjaerts F, Malhotra-
652 Kumar S, Timbermont L, Oliver A, Barraud O, Bellamy T, Bonten M, Goossens H,
653 Reisner C, Esser MT, Jafri HS, The COMBACTE-MAGNET EVADE Study Group,
654 Joannidis M, Klimscha W, De Waele E, Devriendt J, Huberlant V, Depuydt P, Van
655 Boxstael S, Peric M, Kopic J, Hanauer M, Hruby T, Sramek V, Svoboda P, Vymazal T,
656 Novacek M, Annane D, Mira J-P, Souweine B, Dequin P-F, Meziani F, Stephan F,
657 Nseir S, Gibot S, Schwebel C, Plantefeve G, Diehl J-L, Richard C, Lamer C, Klouche
658 K, Jaber S, Zakynthinos E, Filntisis G, Zakynthinos S, Koutsoukou A, Saroglou G,
659 Nikolaou C, Vlachogianni G, Pnevmatikos I, Mandragos K, Kremer I, Rozgonyi ZD,
660 Marjanek Z, Martin-Loeches I, Singer P, Van Heerden V, Carmeli Y, Povoa P, Seoane
661 AA, Moura P, Gonzalez F, Ramirez P, Marti AT, Roca RF, Oteiza L, Escudero D,
662 Piacentini E, Vera P, Tamayo L, Gallego MAG, Canas BS, Figueira I, Leon R, Korten
663 V, Akova M, Wyncoll D, Whitehouse T, Hopkins P, Sim M, Golan Y, Zervos M, Vazquez
664 J, Cherabuddi K, Smulian G, Rouphael N, Welker J, Sims M, Van Duin D, McCarthy
665 T, Polk C. 2022. Safety, efficacy, and pharmacokinetics of gremubamab (MEDI3902),
666 an anti-Pseudomonas aeruginosa bispecific human monoclonal antibody, in P.
667 aeruginosa-colonised, mechanically ventilated intensive care unit patients: a
668 randomised controlled trial. *Crit Care* **26**:355. doi:10.1186/s13054-022-04204-9

669 Chen VB, Arendall WB, Headd JJ, Keedy DA, Immormino RM, Kapral GJ, Murray LW,
670 Richardson JS, Richardson DC. 2010. *MolProbity*: all-atom structure validation for
671 macromolecular crystallography. *Acta Crystallogr D Biol Crystallogr* **66**:12–21.
672 doi:10.1107/S0907444909042073

673 Cisz M, Lee P-C, Rietsch A. 2008. ExoS Controls the Cell Contact-Mediated Switch to
674 Effector Secretion in *Pseudomonas aeruginosa*. *J Bacteriol* **190**:2726–2738.
675 doi:10.1128/JB.01553-07

676 Coburn B, Sekirov I, Finlay BB. 2007. Type III Secretion Systems and Disease. *Clin
677 Microbiol Rev* **20**:535–549. doi:10.1128/CMR.00013-07

678 Crowe JE. 2022. Human Antibodies for Viral Infections. *Annu Rev Immunol* **40**:349–
679 386. doi:10.1146/annurev-immunol-042718-041309

680 Dacheux D, Goure J, Chabert J, Usson Y, Attree I. 2001. Pore-forming activity of type
681 III system-secreted proteins leads to oncosis of *Pseudomonas aeruginosa* -infected
682 macrophages. *Molecular Microbiology* **40**:76–85. doi:10.1046/j.1365-
683 2958.2001.02368.x

684 De Melo AG, Morency C, Moineau S. 2024. Virulence-associated factors as targets for
685 phage infection. *Current Opinion in Microbiology* **79**:102471.
686 doi:10.1016/j.mib.2024.102471

687 Derewenda ZS. 2011. It's all in the crystals…. *Acta Crystallogr D Biol Crystallogr*
688 **67**:243–248. doi:10.1107/S0907444911007797

689 Diepold A, Wagner S. 2014. Assembly of the bacterial type III secretion machinery.
690 *FEMS Microbiol Rev* **38**:802–822. doi:10.1111/1574-6976.12061

691 DiGiandomenico A, Keller AE, Gao Cuihua, Rainey GJ, Warrener P, Camara MM,
692 Bonnell J, Fleming R, Bezabeh B, Dimasi N, Sellman BR, Hilliard J, Guenther CM,
693 Datta V, Zhao W, Gao Changshou, Yu X-Q, Suzich JA, Stover CK. 2014. A
694 multifunctional bispecific antibody protects against *Pseudomonas aeruginosa*. *Sci*
695 *Transl Med* **6**. doi:10.1126/scitranslmed.3009655

696 Dortet L, Lombardi C, Cretin F, Dessen A, Filloux A. 2018. Pore-forming activity of the
697 Pseudomonas aeruginosa type III secretion system translocon alters the host
698 epigenome. *Nat Microbiol* **3**:378–386. doi:10.1038/s41564-018-0109-7

699 Duan L, Zhang J, Chen Z, Gou Q, Xiong Q, Yuan Y, Jing H, Zhu J, Ni L, Zheng Y, Liu
700 Z, Zhang X, Zeng H, Zou Q, Zhao Z. 2021. Antibiotic Combined with Epitope-Specific
701 Monoclonal Antibody Cocktail Protects Mice Against Bacteremia and Acute
702 Pneumonia from Methicillin-Resistant Staphylococcus aureus Infection. *JIR* **Volume**
703 **14**:4267–4282. doi:10.2147/JIR.S325286

704 Emsley P, Cowtan K. 2004. *Coot*: model-building tools for molecular graphics. *Acta*
705 *Crystallogr D Biol Crystallogr* **60**:2126–2132. doi:10.1107/S0907444904019158

706 Erskine PT, Knight MJ, Ruaux A, Mikolajek H, Sang NWF, Withers J, Gill R, Wood SP,
707 Wood M, Fox GC, Cooper JB. 2006. High Resolution Structure of BipD: An Invasion
708 Protein Associated with the Type III Secretion System of Burkholderia Pseudomallei.
709 *Journal of Molecular Biology* **363**:125–136. doi:10.1016/j.jmb.2006.07.069

710 Faudry E, Vernier G, Neumann E, Forge V, Attree I. 2006. Synergistic Pore Formation
711 by Type III Toxin Translocators of *Pseudomonas aeruginosa*. *Biochemistry* **45**:8117–
712 8123. doi:10.1021/bi060452+

713 François B, Luyt C-E, Dugard A, Wolff M, Diehl J-L, Jaber S, Forel J-M, Garot D, Kipnis
714 E, Mebazaa A, Misset B, Andremont A, Ploy M-C, Jacobs A, Yarranton G, Pearce T,
715 Fagon J-Y, Chastre J. 2012. Safety and pharmacokinetics of an anti-PcrV PEGylated
716 monoclonal antibody fragment in mechanically ventilated patients colonized with
717 Pseudomonas aeruginosa: A randomized,double-blind, placebo-controlled trial*.
718 *Critical Care Medicine* **40**:2320–2326. doi:10.1097/CCM.0b013e31825334f6

719 Frank DW, Vallis A, Wiener-Kronish JP, Roy-Burman A, Spack EG, Mullaney BP,
720 Megdoud M, Marks JD, Fritz R, Sawa T. 2002. Generation and Characterization of a
721 Protective Monoclonal Antibody to *Pseudomonas aeruginosa* PcrV. *J INFECT DIS*
722 **186**:64–73. doi:10.1086/341069

Gébus C, Faudry E, Bohn Y-ST, Elsen S, Attree I. 2009. Oligomerization of PcrV and LcrV, protective antigens of Pseudomonas aeruginosa and Yersinia pestis. *Journal of Biological Chemistry* **284**:21776. doi:10.1074/jbc.A803146200

Goure J, Broz P, Attree O, Cornelis GR, Attree I. 2005. Protective Anti-V Antibodies Inhibit *Pseudomonas* and *Yersinia* Translocon Assembly within Host Membranes. *J INFECT DIS* **192**:218–225. doi:10.1086/430932

Goure J, Pastor A, Faudry E, Chabert J, Dessen A, Attree I. 2004. The V Antigen of *Pseudomonas aeruginosa* Is Required for Assembly of the Functional PopB/PopD Translocation Pore in Host Cell Membranes. *Infect Immun* **72**:4741–4750. doi:10.1128/IAI.72.8.4741-4750.2004

Guo EZ, Galán JE. 2021. Cryo-EM structure of the needle filament tip complex of the *Salmonella* type III secretion injectisome. *Proc Natl Acad Sci USA* **118**:e2114552118. doi:10.1073/pnas.2114552118

Habenstein B, El Mammeri N, Tolchard J, Lamon G, Tawani A, Berbon M, Loquet A. 2019. Structures of Type III Secretion System Needle Filaments In: Wagner S, Galan JE, editors. Bacterial Type III Protein Secretion Systems, Current Topics in Microbiology and Immunology. Cham: Springer International Publishing. pp. 109–131. doi:10.1007/82_2019_192

Hauser AR. 2009. The type III secretion system of Pseudomonas aeruginosa: infection by injection. *Nat Rev Microbiol* **7**:654–665. doi:10.1038/nrmicro2199

Heinig M, Frishman D. 2004. STRIDE: a web server for secondary structure assignment from known atomic coordinates of proteins. *Nucleic Acids Research* **32**:W500–W502. doi:10.1093/nar/gkh429

Horcajada JP, Montero M, Oliver A, Sorlí L, Luque S, Gómez-Zorrilla S, Benito N, Grau S. 2019. Epidemiology and Treatment of Multidrug-Resistant and Extensively Drug-Resistant Pseudomonas aeruginosa Infections. *Clin Microbiol Rev* **32**:e00031-19. doi:10.1128/CMR.00031-19

Hu Y, Huang H, Cheng X, Shu X, White AP, Stavrinides J, Köster W, Zhu G, Zhao Z, Wang Y. 2017. A global survey of bacterial type III secretion systems and their effectors. *Environmental Microbiology* **19**:3879–3895. doi:10.1111/1462-2920.13755

Imamura Y, Yanagihara K, Fukuda Y, Kaneko Y, Seki M, Izumikawa K, Miyazaki Y, Hirakata Y, Sawa T, Wiener-Kronish JP, Kohno S. 2007. Effect of anti-PcrV antibody in a murine chronic airway Pseudomonas aeruginosa infection model. *European Respiratory Journal* **29**:965–968. doi:10.1183/09031936.00147406

Jain R, Beckett VV, Konstan MW, Accurso FJ, Burns JL, Mayer-Hamblett N, Milla C, VanDevanter DR, Chmiel JF. 2018. KB001-A, a novel anti-inflammatory, found to be

759 safe and well-tolerated in cystic fibrosis patients infected with Pseudomonas
760 aeruginosa. *Journal of Cystic Fibrosis* **17**:484–491. doi:10.1016/j.jcf.2017.12.006

761 Joosten RP, Long F, Murshudov GN, Perrakis A. 2014. The *PDB_REDO* server for
762 macromolecular structure model optimization. *IUCrJ* **1**:213–220.
763 doi:10.1107/S2052252514009324

764 Kabsch W, Sander C. 1983. Dictionary of protein secondary structure: Pattern
765 recognition of hydrogen-bonded and geometrical features. *Biopolymers* **22**:2577–
766 2637. doi:10.1002/bip.360221211

767 Karplus PA, Diederichs K. 2015. Assessing and maximizing data quality in
768 macromolecular crystallography. *Current Opinion in Structural Biology* **34**:60–68.
769 doi:10.1016/j.sbi.2015.07.003

770 Kaufmann SHE, Dorhoi A, Hotchkiss RS, Bartenschlager R. 2018. Host-directed
771 therapies for bacterial and viral infections. *Nat Rev Drug Discov* **17**:35–56.
772 doi:10.1038/nrd.2017.162

773 Kundracik E, Trichka J, Díaz Aponte J, Roistacher A, Rietsch A. 2022. PopB-PcrV
774 Interactions Are Essential for Pore Formation in the Pseudomonas aeruginosa Type III
775 Secretion System Translocon. *mBio* **13**:e02381-22. doi:10.1128/mbio.02381-22

776 La Guidara C, Adamo R, Sala C, Micoli F. 2024. Vaccines and Monoclonal Antibodies
777 as Alternative Strategies to Antibiotics to Fight Antimicrobial Resistance. *IJMS*
778 **25**:5487. doi:10.3390/ijms25105487

779 Laskowski RA, MacArthur MW, Moss DS, Thornton JM. 1993. PROCHECK: a program
780 to check the stereochemical quality of protein structures. *J Appl Crystallogr* **26**:283–
781 291. doi:10.1107/S0021889892009944

782 Lee P, Stopford CM, Svenson AG, Rietsch A. 2010. Control of effector export by the
783 *Pseudomonas aeruginosa* type III secretion proteins PcrG and PcrV. *Molecular*
784 *Microbiology* **75**:924–941. doi:10.1111/j.1365-2958.2009.07027.x

785 Levin MJ, Ustianowski A, De Wit S, Launay O, Avila M, Templeton A, Yuan Y,
786 Seegobin S, Ellery A, Levinson DJ, Ambery P, Arends RH, Beavon R, Dey K, Garbes
787 P, Kelly EJ, Koh GCKW, Near KA, Padilla KW, Psachoulia K, Sharbaugh A, Streicher
788 K, Pangalos MN, Esser MT. 2022. Intramuscular AZD7442 (Tixagevimab–Cilgavimab)
789 for Prevention of Covid-19. *N Engl J Med* **386**:2188–2200.
790 doi:10.1056/NEJMoa2116620

791 Lunelli M, Hurwitz R, Lambers J, Kolbe M. 2011. Crystal Structure of PrgI-SipD: Insight
792 into a Secretion Competent State of the Type Three Secretion System Needle Tip and
793 its Interaction with Host Ligands. *PLoS Pathog* **7**:e1002163.
794 doi:10.1371/journal.ppat.1002163

Matteï P, Faudry E, Job V, Izoré T, Attree I, Dessen A. 2011. Membrane targeting and pore formation by the type III secretion system translocon. *The FEBS Journal* **278**:414–426. doi:10.1111/j.1742-4658.2010.07974.x

McCoy AJ, Grosse-Kunstleve RW, Adams PD, Winn MD, Storoni LC, Read RJ. 2007. *Phaser* crystallographic software. *J Appl Crystallogr* **40**:658–674. doi:10.1107/S0021889807021206

Mirdita M, Schütze K, Moriwaki Y, Heo L, Ovchinnikov S, Steinegger M. 2022. ColabFold: making protein folding accessible to all. *Nat Methods* **19**:679–682. doi:10.1038/s41592-022-01488-1

Montagner C, Arquint C, Cornelis GR. 2011. Translocators YopB and YopD from Yersinia enterocolitica Form a Multimeric Integral Membrane Complex in Eukaryotic Cell Membranes. *J Bacteriol* **193**:6923–6928. doi:10.1128/JB.05555-11

Morrison C. 2015. Antibacterial antibodies gain traction. *Nat Rev Drug Discov* **14**:737–738. doi:10.1038/nrd4770

Mueller CA, Broz P, Cornelis GR. 2008. The type III secretion system tip complex and translocon. *Molecular Microbiology* **68**:1085–1095. doi:10.1111/j.1365-2958.2008.06237.x

Mulangu S, Dodd LE, Davey RT, Tshiani Mbaya O, Proschan M, Mukadi D, Lusakibanza Manzo M, Nzolo D, Tshomba Oloma A, Ibanda A, Ali R, Coulibaly S, Levine AC, Grais R, Diaz J, Lane HC, Muyembe-Tamfum J-J. 2019. A Randomized, Controlled Trial of Ebola Virus Disease Therapeutics. *N Engl J Med* **381**:2293–2303. doi:10.1056/NEJMoa1910993

Murray CJL, Ikuta KS, Sharara F, Swetschinski L, Robles Aguilar G, Gray A, Han C, Bisignano C, Rao P, Wool E, Johnson SC, Browne AJ, Chipeta MG, Fell F, Hackett S, Haines-Woodhouse G, Kashef Hamadani BH, Kumaran EAP, McManigal B, Achalapong S, Agarwal R, Akech S, Albertson S, Amuasi J, Andrews J, Aravkin A, Ashley E, Babin F-X, Bailey F, Baker S, Basnyat B, Bekker A, Bender R, Berkley JA, Bethou A, Bielicki J, Boonkasidecha S, Bukosia J, Carvalheiro C, Castañeda-Orjuela C, Chansamouth V, Chaurasia S, Chiurchiù S, Chowdhury F, Clotaire Donatien R, Cook AJ, Cooper B, Cressey TR, Criollo-Mora E, Cunningham M, Darboe S, Day NPJ, De Luca M, Dokova K, Dramowski A, Dunachie SJ, Duong Bich T, Eckmanns T, Eibach D, Emami A, Feasey N, Fisher-Pearson N, Forrest K, Garcia C, Garrett D, Gastmeier P, Giref AZ, Greer RC, Gupta V, Haller S, Haselbeck A, Hay SI, Holm M, Hopkins S, Hsia Y, Iregbu KC, Jacobs J, Jarovsky D, Javanmardi F, Jenney AWJ, Khorana M, Khusuwan S, Kissoon N, Kobeissi E, Kostyanev T, Krapp F, Krumkamp R, Kumar A, Kyu HH, Lim C, Lim K, Limmathurotsakul D, Loftus MJ, Lunn M, Ma J, Manoharan A, Marks F, May J, Mayxay M, Mturi N, Munera-Huertas T, Musicha P, Musila LA, Mussi-Pinhata MM, Naidu RN, Nakamura T, Nanavati R, Nangia S, Newton P, Ngoun C,

Novotney A, Nwakanma D, Obiero CW, Ochoa TJ, Olivas-Martinez A, Olliaro P, Ooko E, Ortiz-Brizuela E, Ounchanum P, Pak GD, Paredes JL, Peleg AY, Perrone C, Phe T, Phommasone K, Plakkal N, Ponce-de-Leon A, Raad M, Ramdin T, Rattanavong S, Riddell A, Roberts T, Robotham JV, Roca A, Rosenthal VD, Rudd KE, Russell N, Sader HS, Saengchan W, Schnall J, Scott JAG, Seekaew S, Sharland M, Shivamallappa M, Sifuentes-Osornio J, Simpson AJ, Steenkeste N, Stewardson AJ, Stoeva T, Tasak N, Thaiprakong A, Thwaites G, Tigoi C, Turner C, Turner P, Van Doorn HR, Velaphi S, Vongpradith A, Vongsouvath M, Vu H, Walsh T, Walson JL, Waner S, Wangrangsimakul T, Wannapinij P, Wozniak T, Young Sharma TEMW, Yu KC, Zheng P, Sartorius B, Lopez AD, Stergachis A, Moore C, Dolecek C, Naghavi M. 2022. Global burden of bacterial antimicrobial resistance in 2019: a systematic analysis. *The Lancet* **399**:629–655. doi:10.1016/S0140-6736(21)02724-0

Murshudov GN, Skubák P, Lebedev AA, Pannu NS, Steiner RA, Nicholls RA, Winn MD, Long F, Vagin AA. 2011. *REFMAC* 5 for the refinement of macromolecular crystal structures. *Acta Crystallogr D Biol Crystallogr* **67**:355–367. doi:10.1107/S0907444911001314

Nanao M, Ricard-Blum S, Di Guilmi A, Lemaire D, Lascoux D, Chabert J, Attree I, Dessen A. 2003. [No title found]. *BMC Microbiol* **3**:21. doi:10.1186/1471-2180-3-21

Ngo T-D, Plé S, Thomas A, Barette C, Fortuné A, Bouzidi Y, Fauvarque M-O, Pereira De Freitas R, Francisco Hilário F, Attrée I, Wong Y-S, Faudry E. 2019. Chimeric Protein–Protein Interface Inhibitors Allow Efficient Inhibition of Type III Secretion Machinery and *Pseudomonas aeruginosa* Virulence. *ACS Infect Dis* **5**:1843–1854. doi:10.1021/acsinfecdis.9b00154

Painter J, Merritt EA. 2006. *TLSMD* web server for the generation of multi-group TLS models. *J Appl Crystallogr* **39**:109–111. doi:10.1107/S0021889805038987

Pennini ME, De Marco A, Pelletier M, Bonnell J, Cvitkovic R, Beltramello M, Cameroni E, Bianchi S, Zatta F, Zhao W, Xiao X, Camara MM, DiGiandomenico A, Semenova E, Lanzavecchia A, Warrener P, Suzich J, Wang Q, Corti D, Stover CK. 2017. Immune stealth-driven O2 serotype prevalence and potential for therapeutic antibodies against multidrug resistant Klebsiella pneumoniae. *Nat Commun* **8**:1991. doi:10.1038/s41467-017-02223-7

Quinaud M, Chabert J, Faudry E, Neumann E, Lemaire D, Pastor A, Elsen S, Dessen A, Attree I. 2005. The PscE-PscF-PscG Complex Controls Type III Secretion Needle Biogenesis in Pseudomonas aeruginosa. *Journal of Biological Chemistry* **280**:36293–36300. doi:10.1074/jbc.M508089200

Quinaud M, Plé S, Job V, Contreras-Martel C, Simorre J-P, Attree I, Dessen A. 2007. Structure of the heterotrimeric complex that regulates type III secretion needle formation. *Proc Natl Acad Sci USA* **104**:7803–7808. doi:10.1073/pnas.0610098104

Rollenske T, Szijarto V, Lukasiewicz J, Guachalla LM, Stojkovic K, Hartl K, Stulik L, Kocher S, Lasitschka F, Al-Saeedi M, Schröder-Braunstein J, Von Frankenberg M, Gaebelein G, Hoffmann P, Klein S, Heeg K, Nagy E, Nagy G, Wardemann H. 2018. Cross-specificity of protective human antibodies against Klebsiella pneumoniae LPS O-antigen. *Nat Immunol* **19**:617–624. doi:10.1038/s41590-018-0106-2

Roy-Burman A, Savel RH, Racine S, Swanson BL, Revadigar NS, Fujimoto J, Sawa T, Frank DW, Wiener-Kronish JP. 2001. Type III Protein Secretion Is Associated with Death in Lower Respiratory and Systemic *Pseudomonas aeruginosa* Infections. *J INFECT DIS* **183**:1767–1774. doi:10.1086/320737

Sawa, Kinoshita, Inoue, Ohara, Moriyama. 2019. Immunoglobulin for Treating Bacterial Infections: One More Mechanism of Action. *Antibodies* **8**:52. doi:10.3390/antib8040052

Schoehn G, Di Guilmi AM, Lemaire D, Attree I, Weissenhorn W, Dessen A. 2003. Oligomerization of type III secretion proteins PopB and PopD precedes pore formation in Pseudomonas. *EMBO J*. **22**(19):4957-67. doi:10.1093/emboj/cdg499.

Serapio-Palacios A, Finlay BB. 2020. Dynamics of expression, secretion and translocation of type III effectors during enteropathogenic Escherichia coli infection. *Current Opinion in Microbiology* **54**:67–76. doi:10.1016/j.mib.2019.12.001

Simonis A, Kreer C, Albus A, Rox K, Yuan B, Holzmann D, Wilms JA, Zuber S, Kottege L, Winter S, Meyer M, Schmitt K, Gruell H, Theobald SJ, Hellmann A-M, Meyer C, Ercanoglu MS, Cramer N, Munder A, Hallek M, Fätkenheuer G, Koch M, Seifert H, Rietschel E, Marlovits TC, Van Koningsbruggen-Rietschel S, Klein F, Rybniker J. 2023. Discovery of highly neutralizing human antibodies targeting Pseudomonas aeruginosa. *Cell* **186**:5098-5113.e19. doi:10.1016/j.cell.2023.10.002

Tabor DE, Oganesyan V, Keller AE, Yu L, McLaughlin RE, Song E, Warrener P, Rosenthal K, Esser M, Qi Y, Ruzin A, Stover CK, DiGiandomenico A. 2018. Pseudomonas aeruginosa PcrV and Psl, the Molecular Targets of Bispecific Antibody MEDI3902, Are Conserved Among Diverse Global Clinical Isolates. *The Journal of Infectious Diseases*. doi:10.1093/infdis/jiy438

Tickle IJ. 2007. Experimental determination of optimal root-mean-square deviations of macromolecular bond lengths and angles from their restrained ideal values. *Acta Crystallogr D Biol Crystallogr* **63**:1274–1281. doi:10.1107/S0907444907050196

Vacca F, Sala C, Rappuoli R. 2022. Monoclonal Antibodies for Bacterial Pathogens: Mechanisms of Action and Engineering Approaches for Enhanced Effector Functions. *Biomedicines* **10**:2126. doi:10.3390/biomedicines10092126

907 Verove J, Bernarde C, Bohn Y-ST, Boulay F, Rabiet M-J, Attree I, Cretin F. 2012.
908 Injection of Pseudomonas aeruginosa Exo Toxins into Host Cells Can Be Modulated
909 by Host Factors at the Level of Translocon Assembly and/or Activity. *PLoS ONE*
910 **7**:e30488. doi:10.1371/journal.pone.0030488

911 Watson A, Li H, Ma B, Weiss R, Bendayan D, Abramovitz L, Ben-Shalom N, Mor M,
912 Pinko E, Bar Oz M, Wang Z, Du F, Lu Y, Rybniker J, Dahan R, Huang H, Barkan D,
913 Xiang Y, Javid B, Freund NT. 2021. Human antibodies targeting a Mycobacterium
914 transporter protein mediate protection against tuberculosis. *Nat Commun* **12**:602.
915 doi:10.1038/s41467-021-20930-0

916 West SEH, Schweizer HP, Dall C, Sample AK, Runyen-Janecky LJ. 1994.
917 Construction of improved Escherichia-Pseudomonas shuttle vectors derived from
918 pUC18/19 and sequence of the region required for their replication in Pseudomonas
919 aeruginosa. *Gene* **148**:81–86. doi:10.1016/0378-1119(94)90237-2

920 Yaeger LN, Coles VE, Chan DCK, Burrows LL. 2021. How to kill *Pseudomonas* —
921 emerging therapies for a challenging pathogen. *Annals of the New York Academy of*
922 *Sciences* **1496**:59–81. doi:10.1111/nyas.14596

923 Zucker F, Champ PC, Merritt EA. 2010. Validation of crystallographic models
924 containing TLS or other descriptions of anisotropy. *Acta Crystallogr D Biol Crystallogr*
925 **66**:889–900. doi:10.1107/S0907444910020421

926
927

928 # FIGURES

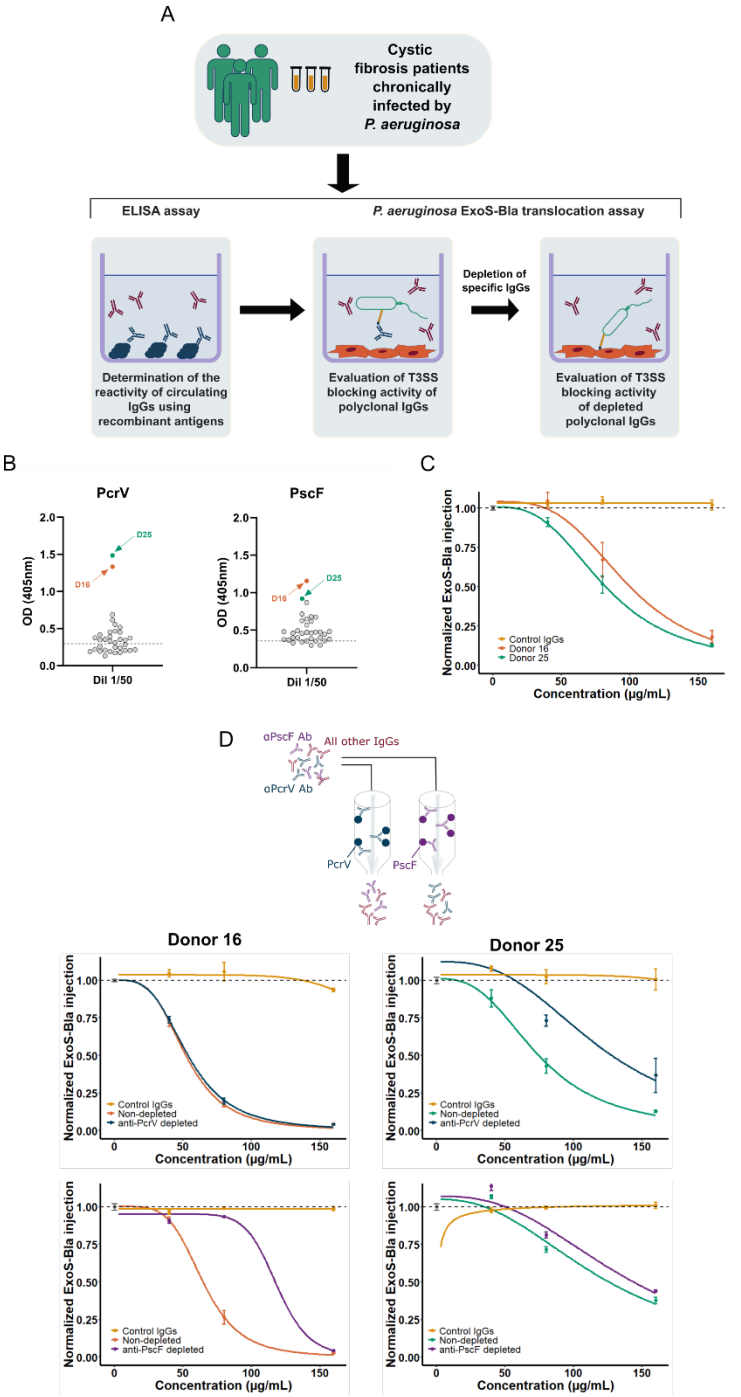

929

930 **Figure 1. Screening workflow and donor selection**

931 (A) Schematic representation of the workflow from patient selection to evaluation of
932 T3SS-blocking activity. (B) ELISA results indicating that sera of donors 16 and 25
933 possess the highest Ab titers against recombinant PcrV and PscF. (C) ExoS-Bla
934 translocation blocking activity of serum from donors 16 and 25. (D) (top) scheme of
935 depletion experiment of specific Abs on either PscF- or PcrV–loaded columns. (bottom)
936 blocking activity of depleted sera for both donors.

A

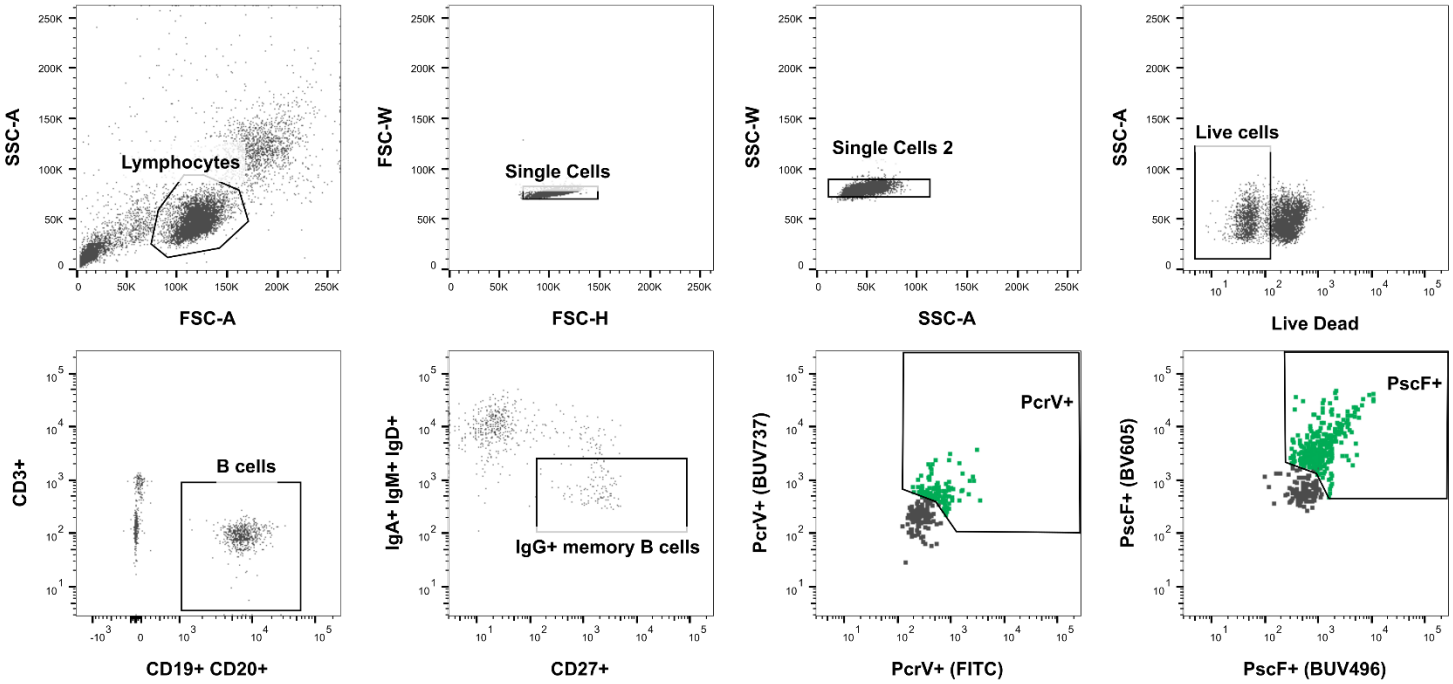

B

Anti-PcrV mAbs	EC_{50} (µg/mL)	ExoS-Bla inhibition
P3D6	0.03	24 %
P5B3	0.04	94 %
P3G9	0.08	No inhibition
P5E10	0.17	No inhibition
Anti-PscF mAbs	**EC_{50} (µg/mL)**	**ExoS-Bla inhibition**
P5G10	0.01	No inhibition
P1B7	0.07	No inhibition
P5D5	0.07	No inhibition
P1D5	0.18	No inhibition
P1B4	0.24	No inhibition
P3G6	1.28	No inhibition
P3G2	2.08	No inhibition
P1F5	4.65	No inhibition
P3G7	10.61	No inhibition
P1D7	>30	No inhibition

Figure 2. Selection of B cells from donors 16 and 25. (A) B cells sorting and isolation using PscF and PcrV baits. (B) Table summarizing the EC_{50} values of selected Abs obtained by ELISA and the percentage of inhibition of ExoS-Bla injection into epithelial cells at 100 µg/mL.

943

A

Variant	Amino acid positions			
	6	9	21	225
V1 (PAO1-like)	Leu	Ala	Ser	Ser
V2 (CHA-like)	Leu	Ala	Ser	Arg
V3 (PA14-like)	Phe	Ala	Pro	Lys
V4 (PA103-like)	Phe	Gly	Pro	Arg
V5	Phe	Gly	Pro	Lys

B

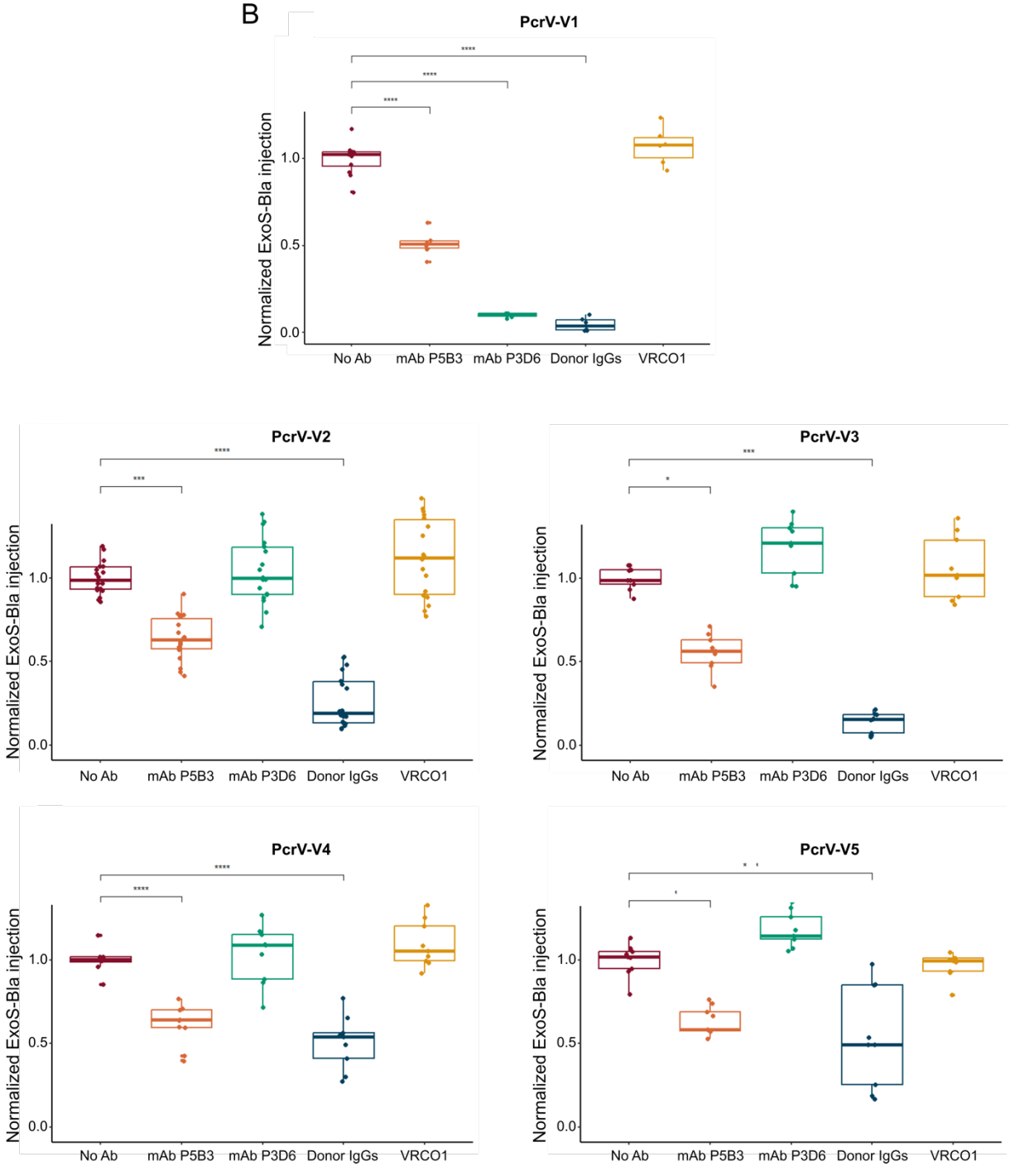

944

945 **Figure 3**. **mAbs P5B3 and P3D6 activity on PcrV variants**. (A) PcrV variability in
946 clinical strains. The most variable position (225) can either be Ser, Arg or Lys.
947 Representative strains are indicated when available (PAO1 for V1, CHA for V2, PA14
948 for V3 and PA103 for V4). (B) Inhibition of ExoS-Bla activity following infection of A549
949 epithelial cells with *P. aeruginosa* expressing the V1 variant. IgGs from donor 25, as
950 well as mAbs P5B3 and P3D6 block ExoS-Bla injection, while the control mAb VRCO1
951 is inefficient. While P3D6 displays significant inhibition only towards V1, P5B3 displays
952 dose-dependent inhibition on all five variants (see also Supplementary Figure 1).

953

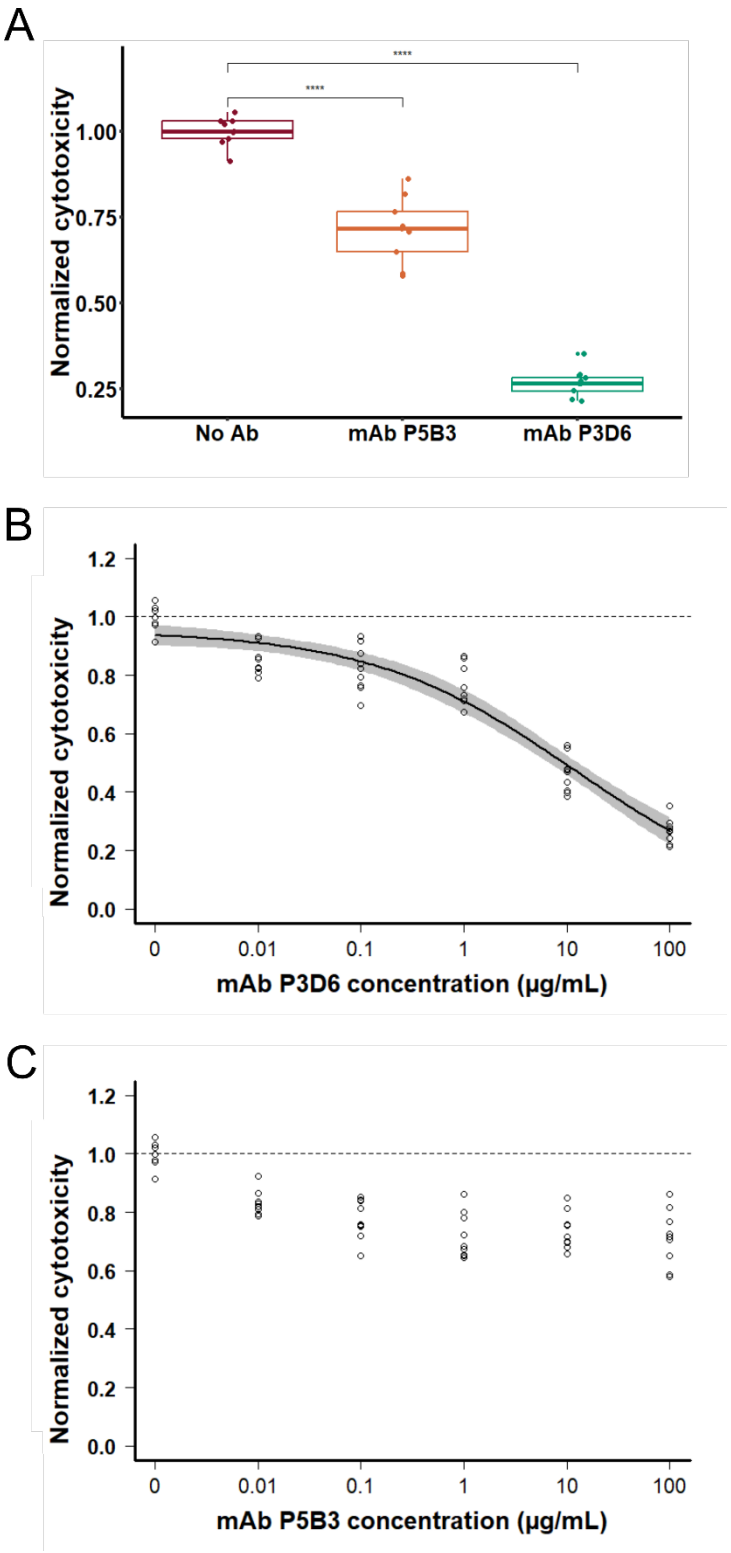

Figure 4. mAb P3D6 efficiently inhibits the PopB/PopD translocation pore. J774 macrophages were infected with *P. aeruginosa* strain (PAO1, V1) deprived of all three T3SS toxins. The cell death (cytotoxicity) resulting from insertion of the translocon pore was measured by propidium iodide incorporation and normalized to the wild-type strain without addition of mAbs. (A) Both P3D6 and P5B3 mAbs significantly reduce pore formation at 100 µg/mL. (B, C) Only P3D6 exhibits a significant dose-response inhibitory effect on cytotoxicity towards J774 cells with an IC_{50} of 11.8 µg/mL.

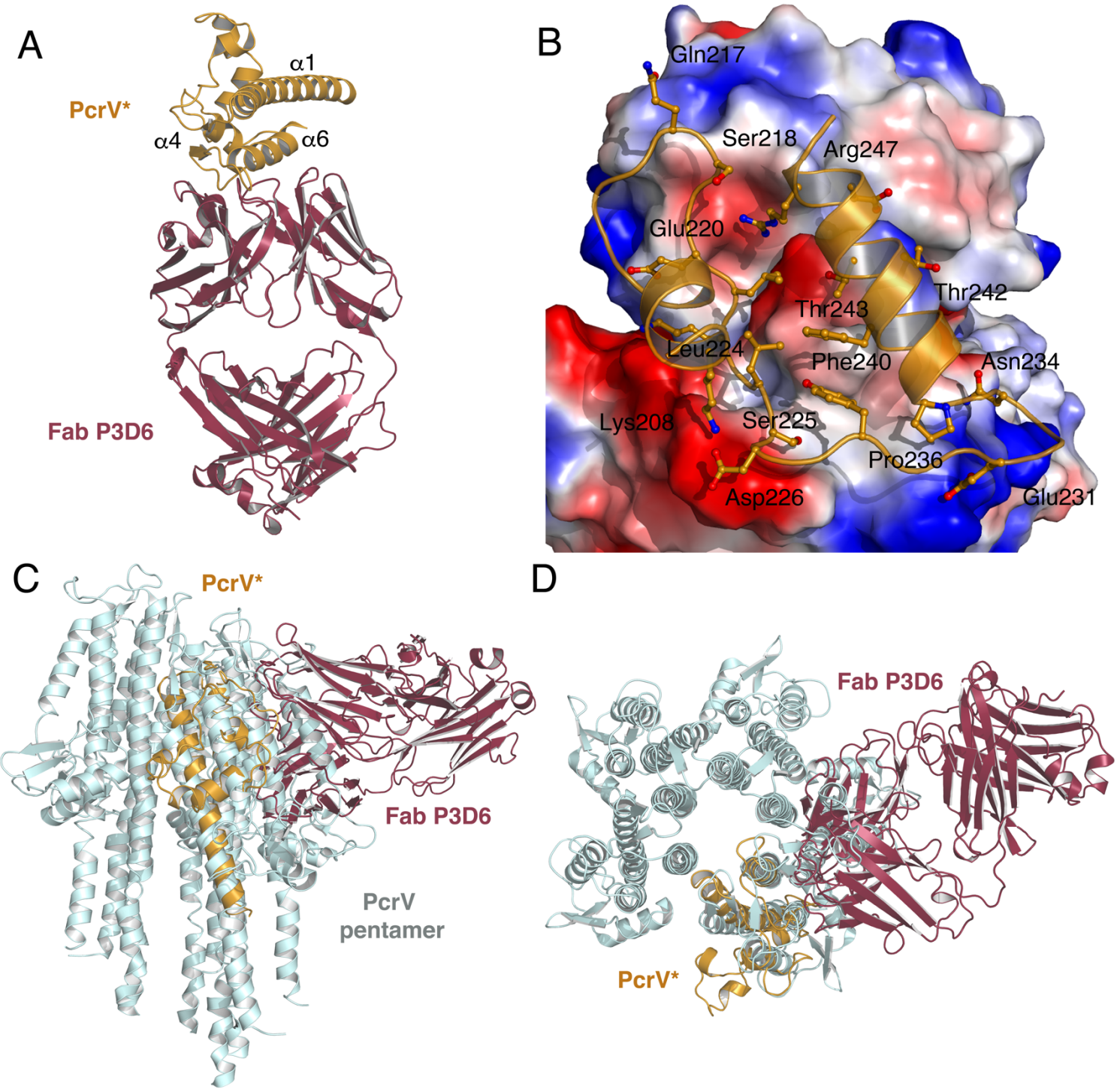

962 **Figure 5. Structure of Fab P3D6 in complex with PcrV***. (A) Crystal structure of Fab
963 P3D6 in complex with PcrV*. Fab P3D6 is shown in brown, while PcrV* is in orange.
964 Contacts are made between PcrV* and an interaction platform formed by both HC and
965 LC of P3D6. (B) Closeup of the interaction between PcrV* and P3D6, with the latter
966 being shown as an electrostatic surface where acidic regions are shown in red, and
967 basic in blue. Side (C) and top (D) views of the modeled PcrV pentamer, in light blue)
968 onto which the structure shown in (A) was overlaid. Note that the bound Fab clashes
969 with a neighboring PcrV protomer, precluding the formation of the pentamer.

970

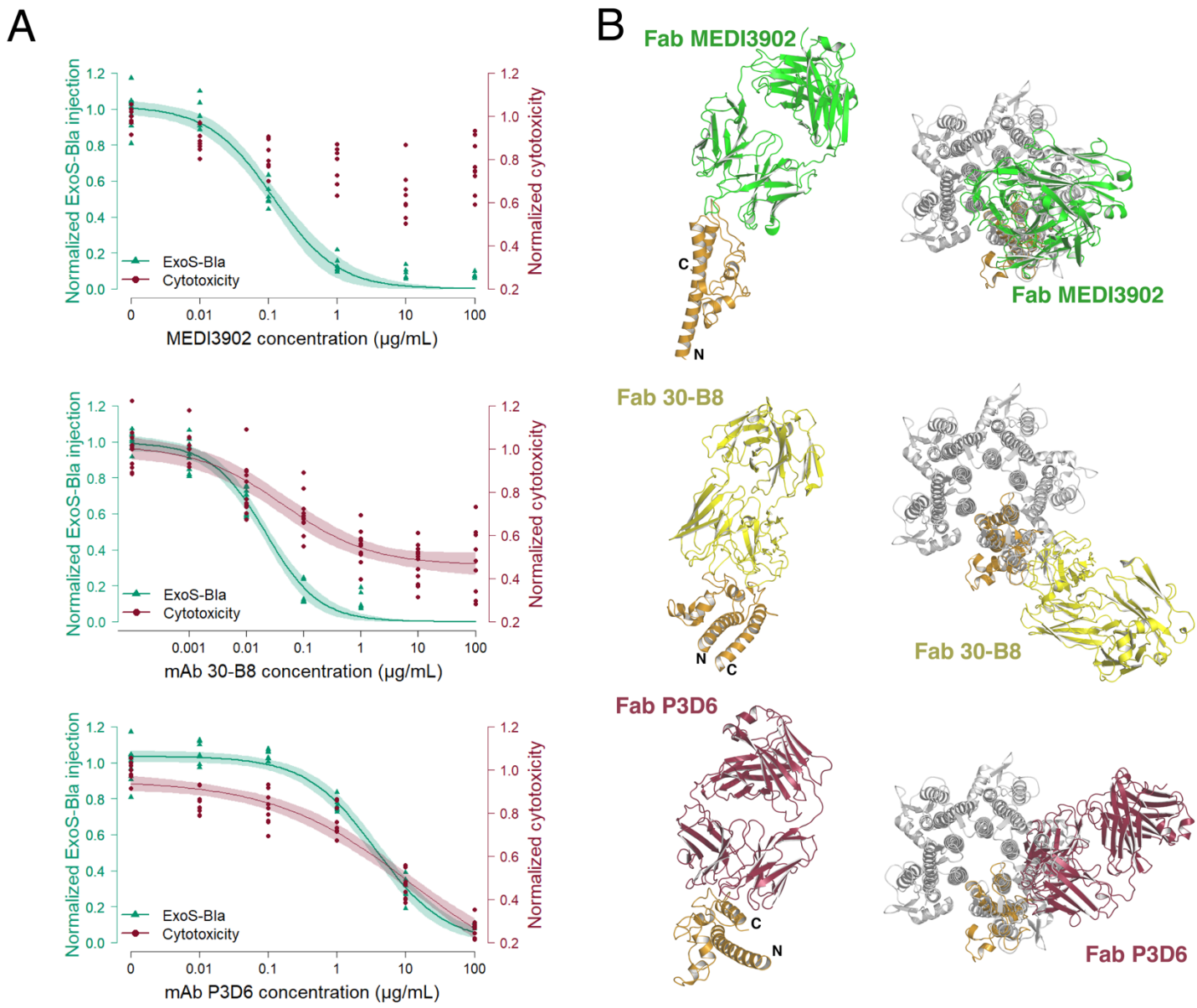

971

972

973 **Figure 6. Functional and structural comparisons between anti-PcrV mAbs.**

974 (A) Dose-dependent inhibition of T3SS in two functional assays reflecting toxin
975 injection (ExoS-Bla injection) and translocon assembly (normalized J774 macrophage
976 cytotoxicity) for three mAbs.

977 (B) Structures of PcrV-Fab complexes in the context of a PcrV monomer, as well as of
978 a pentamer modeled based on the cryo-EM structure of SipD (Guo and Galan 2021).
979 Fab P3D6 binds to a PcrV monomer but clashes with adjacent protomers in the context
980 of the pentamer, while Fab MEDI3902 clashes with other Fab molecules. Fab 30-B8
981 binds to both the PcrV monomer and all pentamer protomers without clashes. N- and
982 C- termini of PcrV are indicated in all structures, which are referenced in the main text.

983

AUTHOR CONTRIBUTIONS

JMD, EF, CCM, FC, LSDD, AA, IB, VTC and FC performed experiments and analyzed the data; EF, CCM and LSDD prepared the figures; DF and YC provided the tools and materials; IA, AD and PP designed the study, analyzed the data, and wrote the manuscript. All authors participated in discussions and editing of the final version of the manuscript.

DECLARATION OF INTERESTS

The authors declare no competing interests.